The Company of Biologists

RESEARCH ARTICLE SPECIAL ISSUE: CELL BIOLOGY OF THE IMMUNE SYSTEM

B cells rapidly target antigen and surface-derived MHCII into peripheral degradative compartments

Sara Hernández-Pérez[1,2,*], Marika Vainio[1,2,*], Elina Kuokkanen[1], Vid Šuštar[1], Petar Petrov[1,2], Sofia Forstén[1,2], Vilma Paavola[1], Johanna Rajala[1], Luqman O. Awoniyi[1,2], Alexey V. Sarapulov[1,2], Helena Vihinen[3], Eija Jokitalo[3], Andreas Bruckbauer[4] and Pieta K. Mattila[1,2,‡]

ABSTRACT

In order to mount high-affinity antibody responses, B cells internalise specific antigens and process them into peptides loaded onto MHCII for presentation to T helper cells (T_H cells). While the biochemical principles of antigen processing and MHCII loading have been well dissected, how the endosomal vesicle system is wired to enable these specific functions remains much less studied. Here, we performed a systematic microscopy-based analysis of antigen trafficking in B cells to reveal its route to the MHCII peptide-loading compartment (MIIC). Surprisingly, we detected fast targeting of internalised antigen into peripheral acidic compartments that possessed the hallmarks of the MIIC and also showed degradative capacity. In these vesicles, internalised antigen converged rapidly with membrane-derived MHCII and partially overlapped with cathepsin-S and H2-M, both required for peptide loading. These early compartments appeared heterogenous and atypical as they contained a mixture of both early and late endosomal markers, indicating a specialized endosomal route. Together, our data suggest that, in addition to in the previously reported perinuclear late endosomal MIICs, antigen processing and peptide loading could have already started in these specialized early peripheral acidic vesicles (eMIIC) to support fast peptide–MHCII presentation.

KEY WORDS: Adaptive immune system, B cells, Antigen processing, B cell receptor, BCR, MHCII, Peptide loading, Endosomes, Vesicle traffic

INTRODUCTION

B lymphocytes (B cells) are an essential part of the adaptive immune system, initiating antibody responses against a vast repertoire of different antigens. The presentation of specific antigen-derived peptides loaded onto the major histocompatibility complex (MHC) class II (MHCII) is critical for the ability of B cells to mount a mature antibody response, including class-switch recombination and affinity maturation. In addition, the presentation of the peptide–MHCII (pMHCII) complex on the B cell surface enables them to act as

antigen-presenting cells (APCs) to CD4+ T lymphocytes (T helper cells, T_H cells). T cell receptor (TCR)–pMHCII interaction provides a second activation signal to the B cells and, reciprocally, pMHCII presented on B cells stimulates cognate T_H cells to orchestrate other branches of the immune system and to generate CD4+ T cell memory (Whitmire et al., 2009).

Presentation of different antigenic peptides on MHCII is a critical driver of various adaptive immune responses. Other professional APCs, such as dendritic cells (DCs) and macrophages, present peptides from antigens taken up unspecifically by phagocytosis or via receptor-mediated uptake by innate immune receptors, like complement receptors or Fc receptors. B cells, however, ensure efficient presentation of antigens of given specificity, as determined by the B cell antigen receptor (BCR) (Aluvihare et al., 1997; Unanue et al., 2016). Studies on pMHCII loading have largely focused on DCs and macrophages, leaving B cell antigen processing and presentation less understood.

The MHCII peptide-loading compartment (MIIC), where antigen is processed into peptides for loading onto MHCII molecules, is characterized by its main hallmarks, antigen and MHCII. In addition, the MIIC contains the key peptide loading chaperone H2-M and the proteolytic enzyme cathepsin-S (CatS) (Adler et al., 2017). The MIIC has been well characterized by various biochemical fractionation techniques. However, in these assays the information about the heterogeneity, localisation and dynamics of the vesicles is typically lost. Therefore, important questions remain about the coordination of antigen processing and MHCII loading and presentation. How the endosomal vesicle machinery of B cells is tuned to enable this highly specific process and how efficient targeting of BCR-bound antigen for processing is coordinated remain unknown. It has been suggested that MIICs are multivesicular and typically contain the late endosome (LE)/lysosome marker late antigen membrane protein 1 (LAMP1) (Adler et al., 2017; Lankar et al., 2002; Unanue et al., 2016). Thus, a picture has been outlined where the maturation of MIIC diverts at the stage of multivesicular bodies (MVBs) before fusion with end-stage lysosome. However, it is not understood how this process is regulated. To help to decipher the molecular underpinnings of antigen presentation, deeper knowledge on intracellular trafficking of antigen is required.

In the past 10–15 years, developments in fluorescence microscopy techniques, including improved fluorophores and fluorescent fusion proteins, as well as more sensitive and higher resolution imaging modalities, have significantly increased our general understanding of intracellular vesicle traffic. Microscopy can provide information about the dynamics and heterogeneity of different vesicle carriers that are otherwise challenging to decipher with other techniques. The classical or ubiquitous endolysosomal pathway is delineated as a route from early endosomes (EEs) to the LE/MVB and, finally, to lysosomes, with early and late recycling endosomes (REs) sending

[1]Institute of Biomedicine, and MediCity Research Laboratories, University of Turku, 20014 Turku, Finland. [2]Turku Bioscience, University of Turku and Åbo Akademi University, 20520 Turku, Finland. [3]Institute of Biotechnology, Electron Microscopy Unit, 00014 University of Helsinki, Finland. [4]Facility for Imaging by Light Microscopy (FILM), National Heart and Lung Institute, Imperial College London, London SW7 2AZ, UK.
*These authors contributed equally to this work

‡Author for correspondence (pieta.mattila@utu.fi)

S.H.P., 0000-0002-0227-1045; P.P., 0000-0001-5551-8032; L.O.A., 0000-0001-7809-3268; A.V.S., 0000-0001-6445-7438; H.V., 0000-0003-3862-9237; E.J., 0000-0002-4159-6934; A.B., 0000-0003-1419-9674; P.K.M., 0000-0003-2805-0686

cargo back to the cell surface. While this general view is relatively well established, new studies continue to reveal dramatic complexity within the endolysosomal system with numerous vesicle sub-populations, transport proteins and vesicle markers, as well as vesicle scission and fusion machineries (Chen et al., 2019; Delevoye et al., 2019; Huotari and Helenius, 2011). A group of vital regulators of vesicle trafficking are the small GTPases of the Rab protein family, which are widely used to define different endolysosomal sub-populations. This family contains more than 60 proteins in humans performing either ubiquitous or specific functions in vesicle trafficking (Wandinger-Ness and Zerial, 2014). The appreciation of the role of the Rab proteins has been key in unravelling endosomal network dynamics. However, different carriers vary not only in terms of their Rab identity markers, but also in size, shape, membrane morphology, subcellular localisation and acidity. In addition, identification of different cell-type-specific variations of vesicular transport systems and diverse specialised endolysosome-related organelles, where the MIIC could be included (Delevoye et al., 2019), pose an ongoing challenge for researchers.

In this work, we set up a systematic microscopy approach to follow how antigen, after BCR-mediated internalisation, traffics to the MIIC. In accordance with previous studies, we detected and quantified gradual clustering of antigen vesicles towards the perinuclear region in 30–60 min. However, immediately after internalisation, antigen was already present in heterogenous vesicles that harboured a mixed selection of both early and late endosomal markers. Interestingly, these early compartments in the cell periphery possessed hallmarks of the MIIC and showed degradative capacity. By specific visualisation of membrane-derived MHCII molecules, we found that in these early antigen compartments, MHCII originated largely from the plasma membrane pool, possibly to support fast, first-wave peptide presentation. This study provides the first in-depth imaging of antigen processing pathway in B cells. We found remarkable efficiency in joint targeting of antigen and membrane-derived MHCII into these peripheral compartments with hallmarks of the MIIC, which we name early MIIC (eMIIC). The results increase our understanding of the endolysosomal machinery responsible for MIIC formation and can facilitate future dissections of the regulation of successful antigen presentation.

RESULTS

### Antigen migrates into the perinuclear area by 30–60 min after activation

To characterise antigen vesicle trafficking in B cells, we first analyse the migration and clustering of antigen in a quantitative manner. We used cultured A20 B cells expressing transgenic D1.3 IgM (A20 D1.3) and activated them with Alexa Fluor-labelled anti-IgM antibodies (AF-αIgM) as surrogate antigen. The localisation of the antigen vesicles was imaged in cells fixed at different time points and stained for pericentriolar material 1 (PCM1) as a marker for the microtubule-organising centre (MTOC) by spinning disc confocal microscopy (SDCM). We found that, within 30–60 min, most cells gathered antigen in a cluster that typically localised quite centrally in the cell, in the vicinity of the MTOC (Fig. 1A), which is highly consistent with the literature (Aluvihare et al., 1997; Siemasko et al., 1998; Tsui et al., 2018; Vascotto et al., 2007a). The same phenomenon was also detected in splenic primary B cells isolated from an MD4 mouse strain, selected for their relatively high and homogenous levels of IgM. Primary B cells, however, showed faster kinetics, with most cells having already accumulated antigen in central clusters in less than 30 min (Fig. 1B). To quantitatively analyse antigen migration, we deconvolved the images to improve

the separation of small vesicles, and then quantified the total number of vesicles per cell and their mean distance to the MTOC with MATLAB-based 3D analysis (Fig. 1C). By showing a reduction in the vesicle number over time, the analysis clearly demonstrated the fusion, or clustering, of vesicles into bigger entities. At the same time, the average distance to the MTOC decreased, depicting migration of the vesicles closer to the MTOC over time (Fig. 1D,E). Although the vesicle number diminished between 30 and 45 min, the mean distance of the vesicles to the MTOC remained constant. This suggested that the majority of the antigen had already been trafficked to the perinuclear region in 30 min, but vesicle fusion events and/or clustering continued at later time points (Fig. 1E). The quantification revealed the overall kinetics of the antigen transition from smaller peripheral vesicles into bigger vesicles or vesicle clusters that accumulate close to the MTOC.

In order to gain insights into the morphological features of the antigen vesicles, we activated the A20 D1.3 cells with a mixture of AF-αIgM and 6-nm-colloidal gold-conjugated anti-IgM and used transmission electron microscopy (TEM) to visualise antigen-containing membrane structures. We found high heterogeneity in the vesicle morphologies, including multivesicular structures, both after 15 min of activation and after 75 min of activation (Fig. 1F; Fig. S1). As MIICs have earlier been characterised as MVB-like structures (Adler et al., 2017; Lankar et al., 2002; Unanue et al., 2016; Vascotto et al., 2007b), the localisation of antigen into multivesicular structures raised a question as to whether at 15 min after activation, in the cell periphery, antigen processing could have already started. At the 75 min time point, the perinuclear area was, in addition to antigen vesicles, very dense in various other membrane organelles, such as Golgi and mitochondria. Consistent with the literature (Vascotto et al., 2007a), we typically found these vesicle-dense areas at sites of nuclear invaginations (Fig. 1F).

Antigen colocalisation with early and late endosomal Rab proteins

Mechanisms of endolysosomal trafficking in various cellular systems are largely governed by the Rab family of small GTPases, which are commonly used to define sub-populations of vesicles with different functions. To reveal the endolysosomal character of the vesicles transporting antigen, we designed a series of co-localisation analyses with the following classical endosomal markers: Rab5 for EEs, Rab7 and Rab9 for LEs and lysosomes, and Rab11 for REs (note that in mammals, there are more than one isoform of the each of these Rab proteins, e.g. Rab5a, Rab5b and Rab5c for Rab5; however, the antibodies used in the immunofluorescence analysis typically recognize several isoforms of each particular Rab protein). As antigen-bound BCR is known to form clusters at the cell membrane prior to endocytosis, we first examined the proportion of the dot-like antigen features that was internalised at the 10–20 min time points, and thus would be expected to colocalise with vesicular markers. At these early time points most vesicles still remain in the cell periphery and it is not readily apparent if the antigen is internalised or just clustered at the plasma membrane. To distinguish the internalised antigen from the antigen still on the plasma membrane, we stimulated the cells with biotinylated AF-αIgM and stained with fluorescent streptavidin (Fig. S2A). We detected that in 10–20 min, ~40–50% of the dotted antigen features in the images represented internalised vesicles, while the rest of the signal originates from antigen that still remains at the cell surface. As expected, at later time points (60 min), the majority of the antigen pool was detected inside the cells (Fig. S2B, C). This was also highly consistent with a flow cytometric analysis
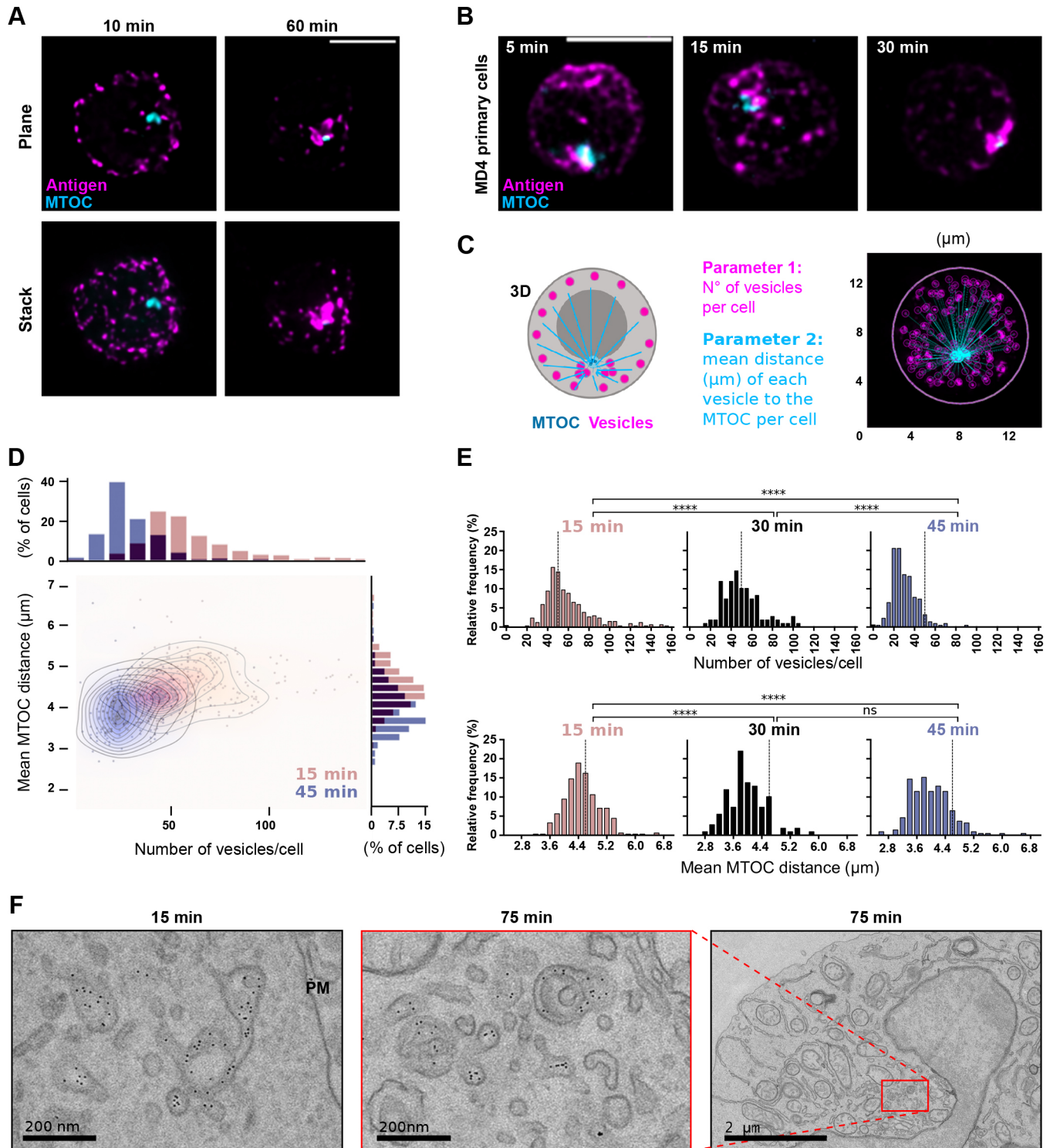
Fig. 1. Antigen vesicles traffic to a perinuclear compartment in the vicinity of the MTOC. (A) A20 D1.3 B cells were activated with Alexa Fluor-labelled anti-IgM antibodies (AF-αIgM) (antigen, magenta) for 10 or 60 min and stained with anti-PCM-1 (to label the MTOC, cyan). Cells were imaged with 3D SDCM and deconvolved. Upper panel, single confocal planes; lower panel, z-projections of 10 μm stacks of representative cells. Scale bar: 5 μm. (B) Primary MD4 B cells were activated with AF-αIgM (antigen, magenta) for different time points and stained with anti-PCM-1 (MTOC, cyan) and imaged as in A. z-projections of the whole stacks from representative cells are shown. Scale bar: 5 μm. (C) Schematic of the vesicle quantification using a MATLAB-based script. Number of antigen vesicles in one cell (in magenta) and mean distance from all the vesicles to the MTOC (in cyan) is measured in a 3D image. Left, schematic representation; right, example image from the script. (D) Quantification of data for experiment shown in A. 3D images from cells activated for 15 (pink) and 45 (blue) min were analysed as in C. Upper axis, mean number of vesicles per cell; right axis, mean distance of the vesicles to MTOC per cell. The two time points were compared using a density plot. (E) Comparison of samples prepared as in A, activated for 15, 30 and 45 min and analysed as in C and D. The dashed lines represent the median of the cell population in the 15 min sample. ****P<0.0001; ns, not significant (Student's t-test). Data for time points 15 and 45 min are for two experiments (n>200 cells) and that for 30 min are for one experiment (n>100 cells). (F) A20 D1.3 cells were activated with anti-IgM conjugated to 6 nm colloidal gold particles mixed with AF647-αIgM, for 15 and 75 min and imaged using TEM. PM, plasma membrane.

of antigen internalisation (Fig. S2D). Consistent with these results, we also frequently found non-internalised antigen at the plasma membrane in TEM samples after 15 min of activation (Fig. S1A).

To study the colocalisation of antigen and different vesicle markers, we performed immunofluorescence analysis with SDCM. We expected to see clearly higher colocalisation of antigen with early endosomal Rab5 in the early time points, and with LE/MVB markers at later time points. To our surprise, we did not detect major differences between the markers. Instead, Rab5, Rab7, Rab9 and Rab11 all showed prominent punctate pattern of vesicles very close to the plasma membrane that partially overlapped with antigen and were partially located just underneath the antigen signal (Fig. 2A,C; Fig. S3A). As a negative control, we used Golgi-specific transport protein Rab6 and, as expected, it showed no notable colocalisation with antigen. We quantified the colocalisation using Manders' overlap coefficient, split for the antigen channel (M2) (Manders et al., 1993), using Huygens software with automated thresholding. M2 measures the portion of antigen that overlaps with the signal from different Rab proteins. The analysis supported that there was already partial colocalisation of antigen with Rab5, Rab7, Rab9 and Rab11 at early time points after activation (Fig. 2C).

At the 60 min time point, when most of the antigen was clustered in the perinuclear region, we found enhanced colocalisation with the LE/MVB markers Rab7 and Rab9, as expected (Fig. 2B; Fig. S3B). Rab11, involved in slow recycling, also localised to the antigen cluster, as well as the EE marker Rab5. The negative control, Rab6, was found in the perinuclear region close to antigen but with very limited overlap in signals. This suggested translocation of the antigen close to the Golgi, supporting the above observed localisation close to the MTOC (Fig. 1). The quantification suggested significant overlap of antigen with all the studied Rab-proteins except Rab6, with an increasing trend over time (Fig. 2C). We also analysed the possible effect of antigen uptake in the distribution of Rab proteins by comparing the intensity of different Rab-positive compartments in the vicinity of the MTOC to the intensity throughout the cell before or 10 and 45 min after activation (Fig. S4A,B). The change in the distribution was most clear in the case of Rab7, which concentrated significantly closer to the MTOC at late time points after activation, accompanied by a decrease in the number of Rab7-positive vesicles (Fig. S4C,D). However, interestingly the distribution of Rab9 did not show any alteration, indicating functional divergence between these two LE/MVB markers. On the other hand, Rab5 and Rab11 showed rather increased dispersion away from the MTOC after 10 min, which could be explained by the activation of the endocytic and exocytic machineries in the case of Rab5 and Rab11, respectively.

The majority of the vesicles were found very close to each other, both at the early and late time points, in the vicinity of the plasma membrane or in the perinuclear region, respectively, leading to overestimation of the signal overlap. The antigen vesicles detected by SDCM, after deconvolution and the analysis by MATLAB script (as in Fig. 1), range between 200 nm and 1 µm in diameter, with a large majority of vesicles falling in between 400 and 500 nm (data not shown). Based on EM micrographs, the actual size of the antigen-containing unilamellar vesicles was, however, found to be ≈120 nm and multilamellar vesicles ≈290 nm (Fig. 1F; Fig. S1A,C), suggesting that the apparent vesicle sizes in fluorescence microscopy are affected by the limited resolution in optical microscopy. Small vesicles located close together are not resolved individually, but appear as one or several larger vesicles. In order to improve the resolution of our data and to better separate different vesicles, with a method still suitable for relatively large sample numbers and

quantification, we employed super-resolution radial fluctuation (SRRF), an imaging method based on post-processing analysis of signal fluctuations (Gustafsson et al., 2016). Here, we analysed samples activated for 10 or 45 min in order to resolve the nature of the antigen vesicles in the perinuclear region. Super-resolution SRRF images were obtained by taking 20–50 repetitive images of the same field of view via SDCM and post-processing the data using the SRRF plugin in ImageJ. In this way, we could improve the separation of the vesicles significantly, and now detected more distinct differences in the localisation of the Rab proteins with respect to antigen, especially at later time points. At 45 min, Rab7 and Rab9 showed clear colocalisation with antigen, as expected for their late endosomal nature, while Rab5 and Rab11 appeared more scattered and only partially colocalised with antigen, often marking vesicles or membrane domains adjacent to it (Fig. 2D; Fig. S5). We analysed SRRF images for the Manders' overlap coefficient (M2) and detected a marked colocalisation of antigen signal with the LE markers Rab7 and Rab9 at 45 min. We also detected overlap with Rab11, and, to some extent, with Rab5. However, in 10 min, the analysis showed close to equal colocalisation of Rab5, Rab7 and Rab9, and a modest level of colocalisation with Rab11. Colocalisation of antigen with Rab6 remained low, confirming the specificity of the analysis (Fig. 2E). The presence of Rab11 in the antigen vesicles could suggest fission and recycling to some extent had already occurred at early time points, but with increasing efficiency towards later time points.

All together, these results point towards a previously unnoticed heterogeneity in the antigen-containing endosomes. Early association of antigen with classical LE/MVB markers Rab7 and Rab9 raises the possibility that antigen vesicles deviate from classical steps of EE to LE conversion during their maturation into the MIIC.

Antigen trafficking involves atypical vesicles that share both early and late endosomal character

To better define antigen transport vesicles, we asked how other typical EE and LE markers, early endosome antigen 1 (EEA1) and LAMP1, respectively, correlated with antigen at different time points. Consistent with the data on different Rab proteins, we detected partial colocalisation of antigen with both EEA1 and LAMP1 already at early time points (Fig. 3A; Fig. S3C). The colocalisation became more prominent as antigen trafficked to the perinuclear region (Fig. 3B; Fig. S3D). Manders' overlap coefficient also showed continuous, or perhaps even increasing, overlap with antigen for both markers (Fig. 3C). However, Pearson's correlation coefficients for EEA1 and LAMP1 crossed over time indicating that a significantly higher proportion of LAMP1 compared to EEA1 colocalised with antigen at later time points. This is consistent with a high proportion of EEA1 endosomes remaining in the cell periphery, while some coalesce in the central cluster together with antigen, as shown by the M2 value. On the other hand, an increasing proportion of LAMP1-positive vesicles accumulated in the perinuclear region with antigen over time.

As a complementary approach, we again turned to SRRF super-resolution analysis in order to achieve higher accuracy. We examined the colocalisation of antigen with EEA1 and LAMP1 at 10 and 45 min after activation. SRRF analysis confirmed higher colocalisation of antigen with EEA1 compared to LAMP1 in the early time points (10 min), and vice versa after 45 min (Fig. 3D,E). Nevertheless, EEA1 colocalisation with antigen was also detected both in some remaining peripheral vesicles and in the perinuclear antigen vesicle cluster, raising a possibility that EEA1 could also
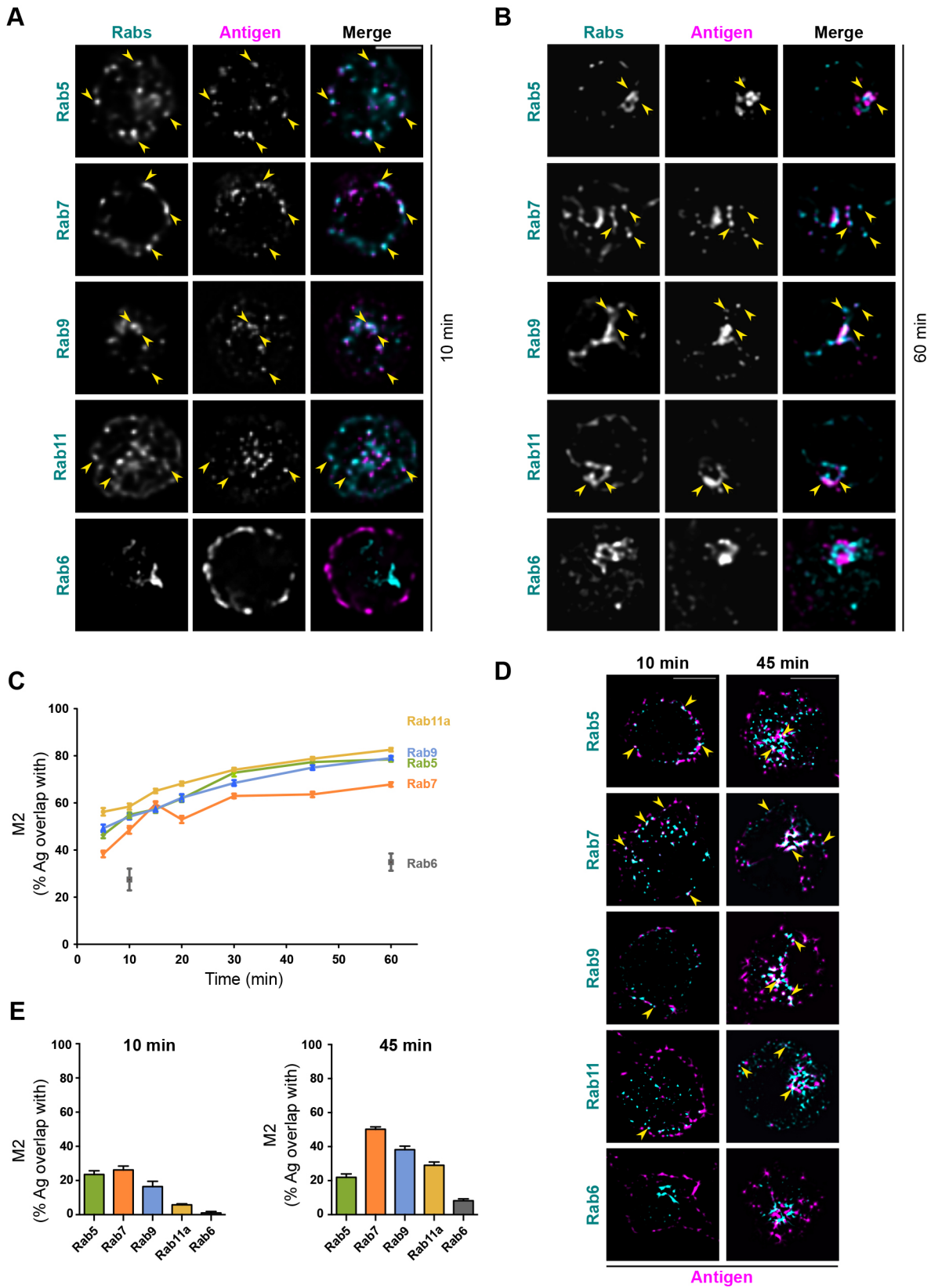
Fig. 2. See next page for legend.

indeed localise to the MIIC. Together, these data revealed surprising localisation of antigen with not only early but also late endosomal carriers shortly after internalisation. At later time points, when vesicles were close to the MTOC, the preference for LE/MVB markers was notable, yet EE markers were also found to overlap with antigen.

Fig. 2. Colocalisation analysis of antigen with different Rab proteins.
(A,B) SDCM imaging of A20 D1.3 cells activated with AF647-αIgM (antigen, magenta) for 10 min (A) or 60 min (B) and immunostained for different Rab proteins (Rab5, Rab7, Rab9, Rab11 and Rab6; cyan). Single confocal planes from deconvolved images of representative cells are shown, and examples of colocalising vesicles are indicated with yellow arrowheads. For clear representation, single confocal planes close to the bottom of the cell are shown for Rab5, Rab7, Rab9 and Rab11. For Rab6, a confocal plane from the middle of the cell, where Golgi is typically located, was selected. See Fig. S3A, B for z-projections. Scale bar: 5 µm. (C) Quantification of the data for experiments as in A and B with additional time points. Antigen (Ag) colocalisation with different Rab proteins was measured from deconvolved images, analysing Manders' overlap coefficients using Huygens. Data from three independent experiments (>80 cells/time point) are shown as mean± s.e.m. (D) Samples were prepared with cells activated for 10 or 45 min as in A, B and imaged with iterative imaging of a single plane with SDCM (20–25 frames/plane) and post-processed to obtain SRRF super-resolution image (antigen, magenta; Rabs, cyan). Examples of colocalising vesicles are indicated with yellow arrowheads. Scale bars: 5 µm. (E) Quantification of the SRRF data for experiments in D, analysing Manders' overlap coefficients with ImageJ. Data shown as mean±s.e.m. Data for the 45 min time point is for two independent experiments and that for 10 min for one experiment (>25 cells/ time point).

As shown above (Fig. S2B,C), in 15 min approximately half of the dots with antigen signal should represent vesicles inside the cell, and the rest should originate from antigen–BCR clusters still at the plasma membrane. Therefore, M2 values for one type of vesicle marker should not be considerably higher than 50% at the early time points. Our observation that antigen showed an overlap of 40–60% with both early and late endosomal markers could simply reflect technical challenges to resolve small vesicles close to each other, causing adjacent vesicles to appear as colocalised. Additionally, it could point towards mixed vesicle identities that would simultaneously possess both types of markers. To test for these two non-exclusive scenarios, we next performed SRRF super-resolution analysis on cells activated either for 10 or 45 min and stained for LAMP1 and EEA1, and asked if they colocalised in the same antigen vesicles. We found vesicles, where antigen only colocalised with either EEA1 or LAMP1, but we also found several prominent vesicles that clearly contained both markers simultaneously (Fig. 3G). To investigate whether this atypical colocalisation was triggered by antigen uptake, we next analysed non-activated cells. Interestingly, we found vesicles with clear EEA1 and LAMP1 colocalisation even in resting cells. The Pearson's coefficient quantification showed lower colocalisation in resting cells as compared to cells activated for 10 min, but comparable colocalisation as in the cells activated for 45 min (Fig. 3F; Fig. S6A). In order to seek for further confirmation for these findings, we also analysed the colocalisation between other pairs of early and late endosomal markers, namely Rab5 and LAMP1, Rab7 and EEA1, and Rab9 and EEA1, before and after activation. In all cases, at the resting state, we can already detect some vesicles with colocalisation, but with very low overall level of correlation, which again, however, increased by 10 min after antigen stimulation (Fig. S6B).

Next, we asked whether the vesicles that share both early and late endosomal markers were in the transition state of their maturation or if they represented a special compartment. To investigate this, we performed live imaging of A20 D1.3 B cells transfected with green fluorescent protein (GFP)-fused Rab5a and loaded with LysoTracker, a fluorescent tracer that labels low pH compartments, such as the LE/MVBs and lysosomes. We followed antigen vesicles at early time points after internalisation by SDCM. We detected several antigen vesicles that contained both Rab5 and LysoTracker

(Fig. 3H; Movie 1). Joint movement of the markers implied physical colocalisation, and indicated that antigen, indeed, traffics in atypical vesicles that share both early and late endosomal features. Interestingly, we also detected double-positive vesicles before cell activation (Fig. S6C).

Antigen enters degradative compartments shortly after internalisation

As the primary purpose of antigen uptake by B cells is to degrade it for loading the resulting peptides onto MHCII complexes, we next asked the question of where and when does the antigen degradation start. We linked a fluorescent probe for proteolysis, DQ–ovalbumin (DQ-Ova), to anti-IgM or specific HEL antigen recognised by the D1.3 BCR (Fig. 4A). Fluorescent DQ moieties quench each other when the probe remains intact. However, upon proteolysis the quenching ceases and the fluorescence can be detected. We first analysed the increase in DQ fluorescence by flow cytometry. We could already detect a clear signal at 15–20 min that constantly increased throughout the 45-min the analysis period, suggesting that the proteolysis starts relatively soon after antigen uptake (Fig. 4B). We detected a brighter DQ-Ova signal at later time points when it was linked to HEL, despite this having similar internalisation rate to anti-IgM (see Fig. S2D). Owing to the brighter signal of DQ-Ova conjugated to HEL, we performed the microscopy analysis using this probe. Fluorescence signal from antigen-linked DQ moieties was also visible by microscopy at 20 min after activation. The DQ-signal overlapped well with EEA1 and was also found to colocalise with CatS, an enzyme essential for preparing the MHCII for peptide loading (Fig. 4C).

To investigate the level of antigen colocalisation with CatS in a more comprehensive way, we performed immunofluorescence analysis in cells activated for 10 or 45 min. Conventional SDCM imaging suggested partial colocalisation of CatS with antigen both at the 10 and 45 min time points (Fig. 4D, upper panel). In order to resolve the vesicles better, we performed SRRF analysis, and could more unambiguously detect antigen vesicles that clearly contained CatS by 10 min after activation (Fig. 4D, middle panel). Interestingly, the colocalisation level remained roughly similar, although low, at the later time points in the perinuclear region (Fig. 4D, bottom panel; Fig. S6D).

Proteolytic activity typically requires that the vesicles have an acidic pH. To examine the pH of the antigen-containing vesicles, we used live imaging with LysoTracker, as its accumulation is based on acidic pH. In line with our data above (Fig. 3H), we already found strong colocalisation of antigen with LysoTracker at the very early time points (1–5 min after activation) (Fig. 4E; Movie 2). Notably, we also detected antigen fusing with LysoTracker-positive vesicles immediately after internalisation, indicating very fast and efficient targeting of antigen to acidic vesicles (Fig. 4F; Movie 3). Curiously, LysoTracker-positive vesicles appeared to 'hover' beneath the plasma membrane ready to catch the internalised antigen.

In addition to LysoTracker, we indirectly studied vesicle pH by analysing the fluorescent decay of FITC coupled to anti-IgM. While Alexa Fluor fluorophores are highly stable at acidic pH, FITC fluorescence is pH-sensitive. A20 D1.3 cells were activated using both AF647-conjugated anti-IgM, as a control, and FITC-conjugated anti-IgM as pH probe, and fluorescence intensities were followed over time by flow cytometry. In agreement with our results using DQ-Ova and fast colocalisation with Lysotracker-positive compartments, we observed a decay in FITC signal already at 5 min after internalisation that continued to further decrease
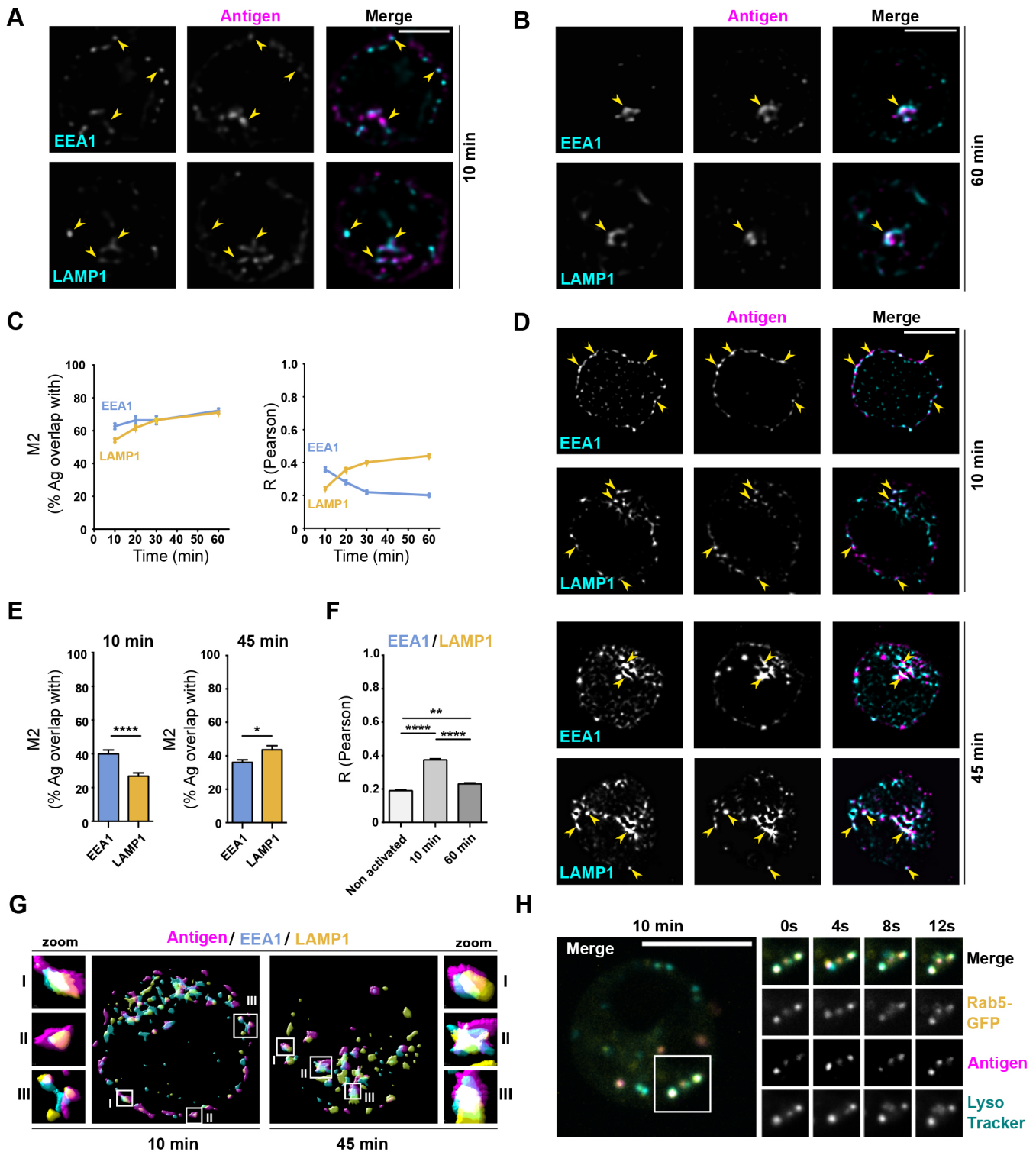
Fig. 3. See next page for legend.

through the experiment (Fig. S6E). In contrast, the AF647 signal remained constant, indicating high stability of the fluorophore.

Antigen colocalises with plasma membrane-derived MHCII rapidly after internalisation

The data above suggests that antigen processing could be initiated in the peripheral antigen vesicles shortly after internalisation. To determine if these early vesicles might represent the MIIC, we asked whether they also contain MHCII. We activated the cells for 10 or 60 min with fluorescent antigen and performed immunofluorescence staining of total MHCII. As expected, we found MHCII to strongly colocalise with antigen in the perinuclear antigen cluster at the 30 min time point. Interestingly, after 10 min of activation, we also detected MHCII in various intracellular vesicles including those containing antigen (Fig. S6F). Owing to the high signal originating from the plasma membrane-resident MHCII and several internal

Fig. 3. Antigen colocalises with both EEA1 and LAMP1 while trafficking to the perinuclear region. (A,B) SDCM imaging of A20 D1.3 cells activated with AF647-αIgM (antigen, magenta) for 10 min (A) or 60 min (B) and immunostained for EEA1 or LAMP1 (cyan). Single confocal planes from deconvolved images; representative cells are shown and examples of colocalising vesicles are indicated with yellow arrowheads. See Fig. S3C,D for z-projections. Scale bars: 5 μm. (C) Quantification of the data for experiments as in A and B with additional time points. Antigen (Ag) colocalisation with EEA1 and LAMP1 was measured from deconvolved images, analysing Manders' overlap coefficients and Pearson's correlation coefficients using Huygens. Data are from two independent experiments (>40 cells/time point) and are shown as mean±s.e.m. (D) Samples were prepared with cells activated for 10 or 45 min as in A and B and imaged with iterative imaging of a single plane with SDCM (20–25 frames/plane) and post-processed to obtain SRRF super-resolution images (antigen, magenta; EEA1 or LAMP1, cyan). Examples of colocalising vesicles are indicated with yellow arrowheads. Scale bar: 5 μm. (E) Quantification of the SRRF data for experiments in D analysing Manders' overlap coefficients with ImageJ. Data from three independent experiments (>30 cells/time point) are shown as mean±s.e.m. (F) Quantification of EEA1 and LAMP1 colocalisation, analysing Pearson's correlation coefficient with Huygens. Data are from three independent experiments (>30 cells/time point) shown as mean±s.e.m. *P<0.05, **P<0.01, ****P<0.0001 (Student's t-test). (G) Surface reconstruction, from the Huygens rendering tool, of SRRF images from samples prepared as in D (antigen, magenta) and immunostained for EEA1 (cyan) and LAMP1 (yellow). Three selected example vesicles are highlighted in the magnification (zoom). (H) A20 D1.3 cells were transfected with GFP–Rab5 (yellow), loaded with LysoTracker (cyan) and activated with RRx–αIgM (antigen, magenta). Live imaging was performed with SDCM (ORCA camera) on a single plane. On the left, a merge image of a representative cell after 10 min of activation is shown. On the right, the region in the white square is followed in each channel as a time-lapse for 12 s, starting 10 min after activation. See Movie 1.

MHCII-positive structures, we decided to analyse the samples with the super-resolution technique structured illumination microscopy (SIM). SIM significantly improved the resolution and clarity of the imaging (x-y-z), and we could detect strong colocalisation of antigen and MHCII in clearly defined vesicles by 15 min after cell activation. We detected extremely high M1 Manders' overlap coefficients in the areas with peripheral antigen vesicles, indicating that almost all internalised antigen overlapped with MHCII. A significant proportion of MHCII was also found with antigen in these regions, as further supported by Pearson's correlation coefficient analysis (Fig. 5A).

To investigate whether the MHCII in the early antigen vesicles was newly synthesised from the trans-Golgi network, or originated from the plasma membrane pool, we pre-labelled the surface MHCII prior to cell activation (Fig. 5B). Interestingly, we saw a strong localisation of surface-derived MHCII (sMHCII) to early antigen vesicles (Fig. 5C). We then proceeded to verify the colocalisation by performing live imaging of cells labelled with fluorescent anti-MHCII antibody prior to activation with fluorescent antigen. The movies revealed very high level of sMHCII in the antigen vesicles (Fig. 5D; Movie 4). Finally, to further prove that the early antigen vesicles could function as the MIIC, we stained the cells for H2-M, a molecule of MHC family that functions as a key chaperone in peptide loading to MHCII (Mellins and Stern, 2014). Notably, SRRF super-resolution imaging of immunofluorescence samples revealed that there already was clear colocalisation of antigen vesicles and H2-M at 15 min after activation further supporting classification of these vesicles as eMIICs (Fig. 5E; Fig. S6D).

Finally, to examine the functionality of eMIICs in peptide loading, we utilised a well-stablished 3,3′ diaminobenzidine-peroxidase (DAB-HRP) endosome ablation technique combined with an ELISA-based antigen presentation assay. Monomeric DAB is polymerised in the presence of H_2O_2 and HRP, selectively fixing

the HRP-containing endosomes by crosslinking the luminal and membrane integral proteins of the vesicles (Henry and Sheff, 2008; Pond and Watts, 1999; Stoorvogel et al., 1996). We pulsed A20 D1.3 cells with HRP-labelled anti-IgM antibody (HRP-αIgM) for 10, 20 or 45 min followed by DAB ablation of the HRP-αIgM-containing endosomal compartments. Then, we activated the endosome-ablated A20 D1.3 cells with HEL antigen. By using a cognate T cell line, 1E5, that recognises HEL-derived peptides on I-A^d, the particular type of MHCII expressed by the A20 D1.3 B cells, we were able to measure IL-2 secretion by T cells as an antigen presentation readout. We found normal levels of peptide presentation when HRP-αIgM vesicles were ablated after 10 min, and close to normal levels after 20 min activation. At these time points, however, only a fraction of the antigen is internalised (Fig. S2D), and the cells continue internalising antigen and are likely to have remaining endosomal capacity for trafficking. This indicates that, even if all HRP-αIgM endosomes are ablated at these time points, a pool of early carriers still remains functional. Interestingly, we also detected robust presentation, at 60% compared to the non-treated cells, in cells where HRP-αIgM vesicles were ablated after 40 min. At this time point, most of the antigen has been internalised and reached the perinuclear MIICs (see Fig. 1 and Fig. S2D). This result suggests that the perinuclear MIICs are not fundamentally required for presentation but the eMIIC could also generate pMHCII to support pMHCII generation. Nevertheless, it is also possible that the DAB-HRP reaction does not completely abolish all perinuclear MIICs, or that they are regenerated during the second activation maturing from a non-ablated endosomal pool.

DISCUSSION

To the study vesicular networks responsible for antigen processing in B cells, we utilised high and super-resolution microscopy for systematic colocalisation analysis of antigen with key markers of various endolysosomal compartments and known components of MIIC. Consistent with previous studies (Aluvihare et al., 1997; Siemasko et al., 1998; Vascotto et al., 2007a), we observed that, over time, antigen concentrates in the perinuclear region together with the LE/MBV markers LAMP1, Rab7 and Rab9, in compartments closely fitting the description of the MIIC. However, we also observed fast and highly efficient targeting of antigen into acidic compartments that also possessed key features of MIIC by minutes after internalisation. These vesicles, located in the cell periphery, displayed a heterogenous combination of early and late endosomal markers and also exhibited variable ultrastructural morphologies. Interestingly, we show robust recruitment of surface-derived MHCII to these compartments, which we named eMIICs, suggesting that they could support fast presentation using MHCII recycled from the plasma membrane (Fig. 6). This work provides the first endosomal roadmap of the intracellular trafficking of antigen in B cells and reveals previously unappreciated efficacy in MIIC formation.

Much of our knowledge on B cell antigen processing compartments is derived from biochemical studies, including cell fractionations, radiolabelling of antigen and electron microscopy (Amigorena et al., 1994; Lankar et al., 2002; West et al., 1994). While these early studies had already drawn a valid picture of late endosomal or lysosomal (i.e. LAMP1-positive), and multivesicular compartment, the approaches were not suitable to address questions about intracellular localisation or dynamics of the antigen vesicles. However, these features have been strongly linked to distinct functional properties of endolysosomes and they also inform us about the possible molecular machineries regulating vesicle trafficking (Huotari and Helenius, 2011; Hutagalung and Novick,
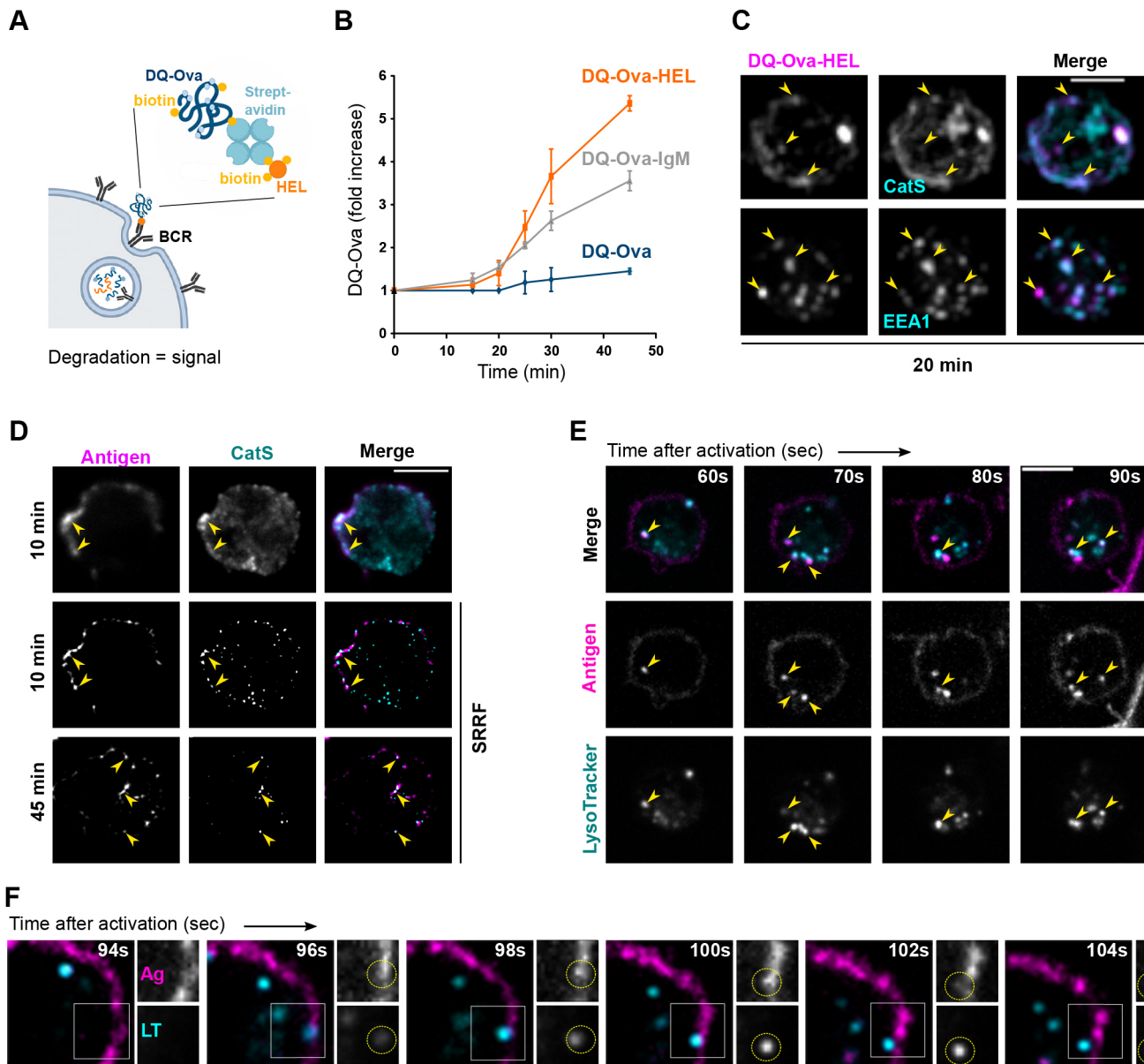
Fig. 4. Internalised antigen incorporates into vesicles with low pH and capability to degrade cargo. (A) Schematic view of the DQ-Ova–antigen (HEL) sandwich used to probe proteolysis of antigen internalised by the BCR. (B) DQ-Ova and DQ-Ova–antigen (αIgM or HEL) degradation as assessed by flow cytometry. Cells were labelled as in A, washed, and incubated for different times at 37°C, and the fluorescence of DQ-OVA was acquired immediately. Results are shown as fold increase (mean±s.d. of the DQ-OVA intensity, normalised to the intensity at time zero). n>2 independent experiments. (C) A20 D1.3 cells activated with DQ-Ova–HEL (magenta) as in B, for 20 min, were immunostained for EEA1 or CatS (cyan). Images were acquired using SDCM with the EVOLVE (EMCCD) camera. z-projections of representative cells (n=3 independent experiments) are shown with examples of colocalising vesicles indicated with yellow arrowheads. Scale bar: 5 μm. (D) A20 D1.3 cells activated with AF647-αIgM (antigen, magenta) for 10 or 45 min and immunostained for CatS (cyan) were imaged with conventional SDCM (upper panel, single plane) or with iterative imaging to obtain SRRF super-resolution images (20–25 frames/plane) (middle and bottom panels). Examples of colocalising vesicles are indicated with yellow arrowheads. Scale bar: 5 μm. (E,F) A20 D1.3 cells were loaded with LysoTracker (cyan) and activated with AF488 F(ab′)2-αIgM (antigen, magenta). Live imaging was performed with SDCM with the EVOLVE (EMCCD) camera every 2 s (E) or 500 ms (F), starting as soon as possible after transition of the cells to 37°C under the microscope. (E) A time-lapse from a representative cell is shown and examples of colocalising vesicles are indicated with yellow arrowheads. Scale bar: 5 μm. See Movie 2. (F) A time-lapse of an example movie highlighting a probable fusion event between an internalising antigen (Ag) vesicle and a LysoTracker (LT)-stained vesicle (dashed yellow circle). A white square in the merge image (left) depicts the region shown for the single channels in the right-hand panels. See Movie 3.

2011). Our microscopy analysis revealed a remarkable heterogeneity in the endolysosomal markers of antigen vesicles (Figs 1–3). However, the overlapping fluorescent signals could have been derived from a vesicle containing two markers, two vesicles containing different markers, or a multilobular vesicle with distinct markers in different domains, and these distinct conditions cannot be resolved by conventional light microscopy. Therefore, the small size and crowdedness of the vesicles generated challenges for the colocalisation analyses, particularly affecting the calculation of the Manders' overlap coefficient, which relies on area overlap. We could, at least partially, overcome this limitation by performing super-resolution SRRF and SIM analyses. While SDCM can
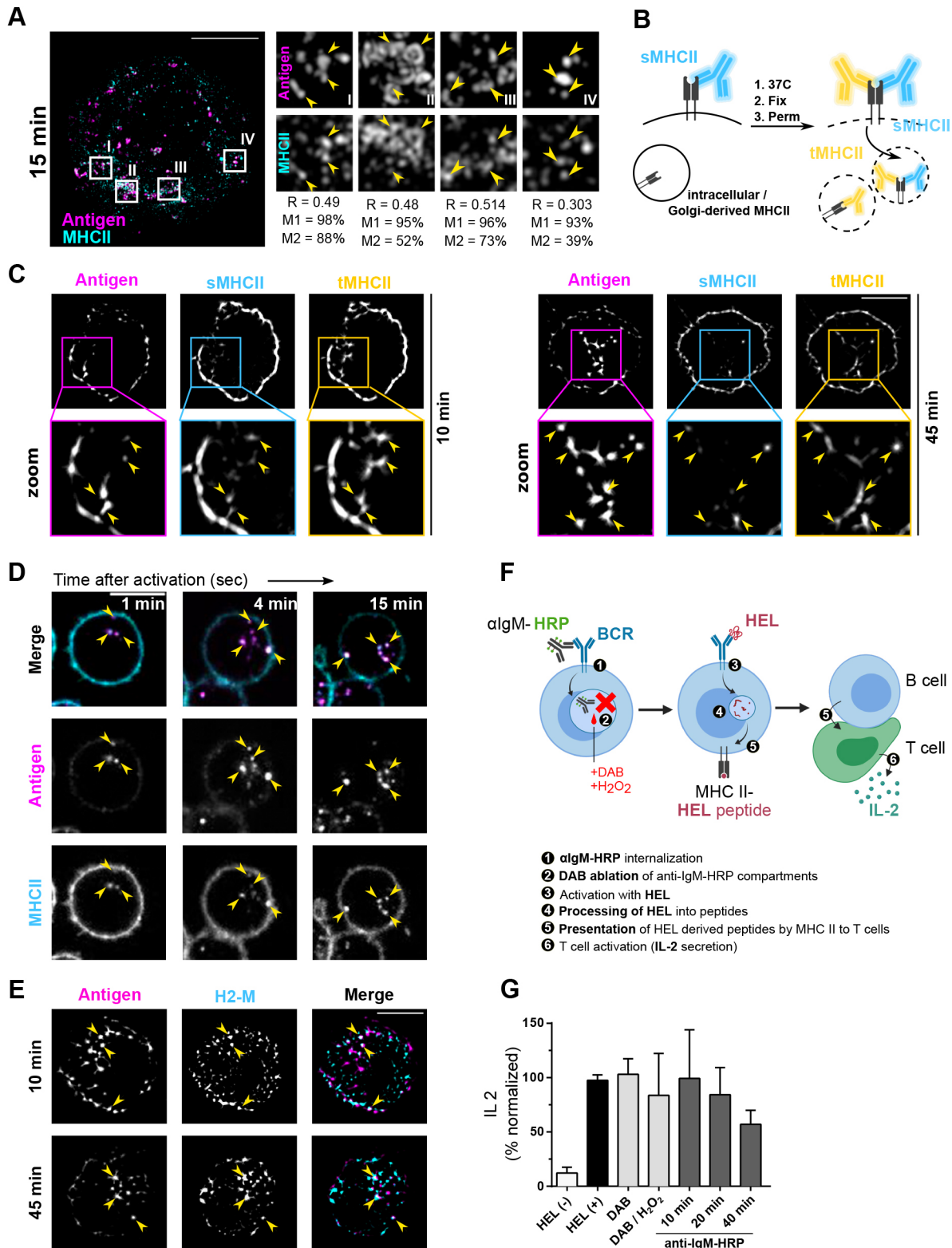
Fig. 5. See next page for legend.

achieve a lateral resolution of 250–300 nm, SIM and SRRF improve the *x-y* resolution by ∼2-fold. SIM also improves the axial resolution by 2-fold from ∼600 to ∼300 nm.

The vesicle heterogeneity could be linked to the notion that antigen enters vesicles with low pH (indicated by LysoTracker and

fast decay of FITC fluorescence) and degradative capacity (demonstrated by DQ-Ova signal and partial overlap with CatS) extremely fast after internalisation (Fig. 4). It has also been shown that the amounts of Rab-proteins on a given vesicle can fluctuate, increasing the noise in the colocalisation parameters (Huotari and

Fig. 5. Antigen and surface-derived MHCII rapidly converge after internalisation. (A) SIM imaging of A20 D1.3 cells activated with AF647-αIgM (antigen, magenta) for 15 min and immunostained for MHC-II (cyan). A representative cell (stack image with 0.125 μm step size) is shown on the left with white squares indicating the regions shown as I–IV (1.6 μm×1.6 μm) on the right. Quantification of each region is shown below as: M1 (Manders' coefficient 1; percentage colocalisation of antigen with MHCII), M2 (Manders' coefficient 2; percentage colocalisation of MHCII with antigen) and R (Pearson's correlation coefficient). Scale bar: 5 μm. (B) A schematic view on the staining to distinguish surface-derived MHCII from the total pool, used in C and D. (C) A20 D1.3 cells (plane image; antigen in magenta) were stained with anti-MHCII (AF488) before activation with RRx-αIgM (antigen, magenta) to label surface-bound MHCII (sMHCII, cyan). After activation for 10 or 45 min at 37°C, cells were fixed and permeabilised and stained with anti-MHCII and a secondary antibody (AF633; tMHCII, yellow). Samples were imaged with iterative imaging of a single plane with SDCM (20–25 frames/plane) and post-processed to obtain SRRF super-resolution images. Upper panel: representative cell; lower panel, magnification of the region shown by the coloured square in the upper panel. Examples of colocalising vesicles are indicated with yellow arrowheads. Scale bar: 5 μm. (D) Live imaging of A20D1.3 stained on ice with AF488-anti-MHCII (cyan) and RRx-αIgM (antigen, magenta). Samples were imaged every 5 s using SDCM after 1 min at 37°C (ORCA camera). A time-lapse from a representative cell is shown, and examples of colocalising vesicles are indicated with yellow arrowheads. Scale bar: 5 μm. See Movie 4. (E) SRRF imaging of A20 D1.3 cells activated with AF647-αIgM (antigen, magenta) for 10 or 45 min and immunostained for H2-M (cyan). A representative cell is shown and examples of colocalising vesicles are indicated with yellow arrowheads. Scale bar: 5 μm. (F) A schematic illustration explaining the experimental process of DAB-mediated endosome ablation and antigen presentation to T cells. (G) Effect of DAB-mediated endosome ablation on antigen presentation measured as IL-2 secretion by ELISA, as schematically illustrated in F. HEL (−): negative control, untreated A20 D1.3 cells without antigen. HEL (+): positive control, untreated cells activated with HEL. DAB: cells treated with DAB and HRP (without H_2O_2) and activated with HEL. DAB/H_2O_2: cells treated with DAB and H_2O_2 (without HRP) and activated with HEL. anti-IgM-HRP: cells activated with HRP-αIgM for different time points, treated with DAB and H_2O_2 and activated with HEL. Results are mean±s.d. (n=3) and are shown as percentage of IL-2 secretion compared to that in the control cells [HEL(+), set at 100%].

Helenius, 2011; Hutagalung and Novick, 2011; Rink et al., 2005; Vonderheit and Helenius, 2005). Notably, we found that antigen also trafficked in atypical vesicles stably marked by both early endosomal Rab5 and LysoTracker indicating that the heterogeneity of the vesicles would be a more constant feature and not a mere transition state. Our data do not clearly fit the classical 'Rab conversion' model, where a vesicle rapidly shifts from being Rab5 positive into being Rab7 positive (Huotari and Helenius, 2011; Hutagalung and Novick, 2011). Instead, the data might better comply with an alternative model, where sequential budding of membrane domains with LE markers would occur from EE/sorting endosomes (Huotari and Helenius, 2011; Wandinger-Ness and Zerial, 2014) and, indeed, we often detected adjacent localisation of different markers possibly indicative of distinct domain on the same vesicle.

Martinez–Martin and colleagues used SIM to demonstrate, in primary B cells, that 15 min after activation, part of the internalised antigen concentrated in ring-like structures representing autophagosomes (Martinez-Martin et al., 2017). However, it remains unclear what could be the role of autophagy in terms of antigen fate or pMHCII processing. In our SIM analysis, we also detected some ring-like structures, which could represent autophagosomes (Fig. 5A) and the partial partitioning of antigen in these autophagosomes, or amphisomes, could explain some of the vesicle heterogeneity we observed. Our data also does not rule out contribution of other vesicular carriers, like clathrin-independent carriers (CLICs), void of specific markers (Kirkham et al., 2005).

An interesting finding from our live imaging data was that the LysoTracker-positive (i.e. low pH) vesicles, appeared to 'hover' close to the plasma membrane and capture antigen right after internalisation (Fig. 4F). Some of these LysoTracker-positive vesicles also already contained Rab5 before cell activation (Fig. S6C). The overexpression of Rab proteins has some caveats and Rab5–GFP can, for instance, lead to the generation of enlarged EEs and only partially recapitulate the behaviour of endogenous Rab5. We, however, also stained B cells for different pairs of endogenous early and late endosomal markers, and consistently found indications of colocalisation of both markers, especially in early stages after cell activation but to some extent already prior to cell activation (Fig. 3F; Fig. S6). This effectiveness suggests prewiring of the B cells endolysosomal system towards antigen presentation, accompanied or boosted by a signalling component from the BCR, as indicated by our analysis in steady-state versus activated cells (Fig. S6) and as suggested previously by Siemasko and colleagues (Siemasko et al., 1998). As such, we support MIIC to be considered as a member of the growing family of specialised endolysosome-related organelles (ELRO) with diverse functions, as proposed in a recent review by Delevoye and colleagues (Delevoye et al., 2019). Considering the poor compliance of antigen vesicles with classical endolysosomal pathway, other ELROs could serve as valuable additional points of comparisons for studies of MIIC membrane trafficking. It has been shown that B cells on activatory surfaces mimicking immunological synapses, polarise the MTOC and acidic MHCII vesicles leading to the secretion of proteases for antigen extraction (Yuseff et al., 2011). While this happens at later stages of activation and is proposed to precede antigen internalisation, it demonstrates atypical functions of B cell acidic compartments, perhaps analogous to the secretion of lytic granules, another type of ELRO, by CD8+ T cells (Delevoye et al., 2019; Yuseff et al., 2013).

Early biochemical studies, using lipopolysaccharide-activated B lymphoblasts, have proposed the existence of peptide-loaded MHCII in multiple endolysosomal compartments (Castellino and Germain, 1995) and, using the same B cell line as us, demonstrated that B cells can indeed already present antigen at 20 min after activation (Aluvihare et al., 1997). Furthermore, studies have shown antigen degradation into peptides 20 min after activation (Barroso et al., 2015; Davidson et al., 1990). These studies are consistent with our finding that the internalised antigen vesicles highly efficiently colocalise with MHCII in various compartments, as well as partially overlap with CatS and H2-M (Figs 4 and 5). The acidic nature and degradative capacity of the eMIICs (Figs 4 and 5) further supports the idea that these compartments have a function in antigen processing, which is also suggested by robust pMHCII presentation detected in the cells where late perinuclear MIICs were ablated with a DAB-HRP reaction (Fig. 5F).

Interestingly, we found that the newly internalised antigen robustly colocalised with surface-derived MHCII (Fig. 5), suggesting that the pre-existing pool of MHCII could be used for the first wave of pMHCII presentation. This point has been previously tested using cycloheximide, known to block *de novo* protein synthesis. There, however, cycloheximide was found to inhibit all presentation and it was interpreted that B cells could only present peptides on newly synthesised MHCII (Aluvihare et al., 1997). Later, concerns have been raised on the side effects of cycloheximide. These include disturbance of vesicle trafficking, actin cytoskeletal dynamics and cell polarisation and motility (Clotworthy and Traynor, 2006; Darvishi and Woldemichael, 2016; Oksvold et al., 2012). Thus, the early findings with cycloheximide warrant revisiting with a sensitive pulse assay for antigen presentation together with more specific inhibitors like, for
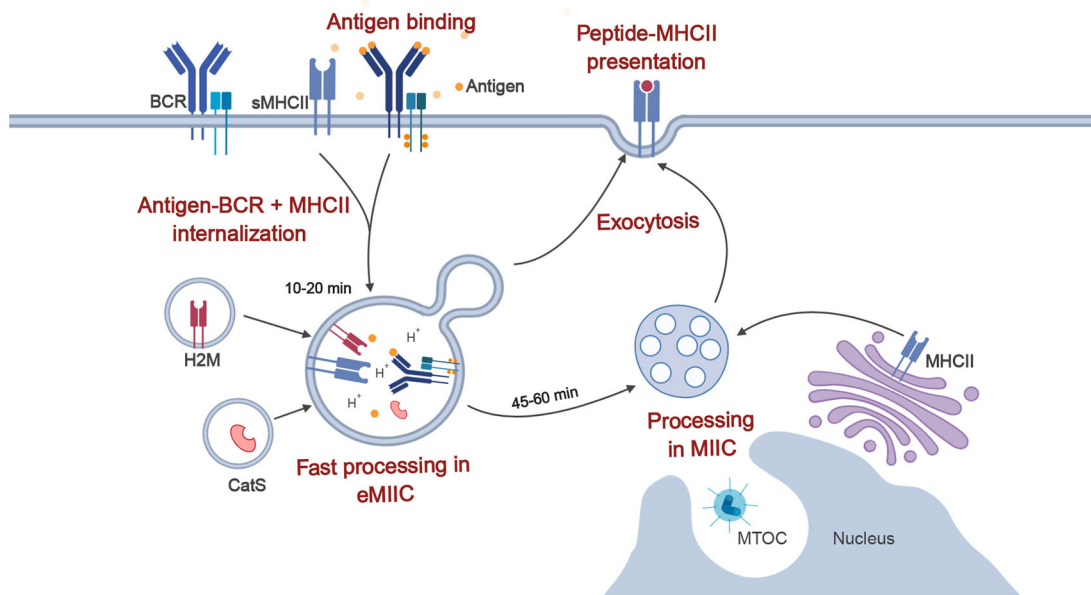
Fig. 6. Model of antigen processing in B cells. B cells internalise antigen and surface MHCII (sMHCII) and target them to early MHCII compartments (eMIIC) to support fast antigen processing and pMHCII presentation. At later stages, antigen is targeted to classical MIIC compartments in the perinuclear region for further pMHCII presentation.

example, the newly developed FLI-06 that targets ER exit sites and the trans-Golgi network (Yonemura et al., 2016). Our suggestion that biosynthetic MHCII probably arrives to MIIC at later stages, is supported by the early metabolic labelling studies, where, again using the same B cell line as that in our study, it was shown that the newly synthesised MHCII arrives to MIIC in 30–60 min after cell activation (Amigorena et al., 1994).

eMIICs could facilitate the speed of pMHCII presentation but could also tune the peptide repertoire. In cell fractionation studies, the MHC class II-like protein H2-O has been reported to concentrate more with the EE fraction as compared to the LE fraction, while the peptide-loading chaperone H2-M shows the opposite trend (Gondré-Lewis et al., 2001). While H2-O has been characterised as having an inhibitory effect on H2-M, it has also been shown to modulate the repertoire of peptides presented on MHCII via unclear mechanisms (Denzin et al., 2005; Karlsson, 2005). Owing to lack of working antibodies for mouse cells, we were not able to analyse H2-O in our system. Nevertheless, H2-O has been shown to dissociate from H2-M at an acidic pH, thereby releasing the inhibition of peptide loading by H2-M (Jiang et al., 2015). This mechanism would allow peptide loading even in the presence of H2-O. Different ratios of H2-M and H2-O could thus distinguish the peptides sent out from eMIICs from those originating from mature MIICs.

By using TEM, we found antigen in vesicles with diverse morphologies (Fig. 1F, left; Fig. S1A). Various compartments, ranging from spherical to multilobular, harboured intralumenal vesicles, consistent with reports characterising MIICs with multivesicular features (Roche and Furuta, 2015; Unanue et al., 2016; van Lith et al., 2001; Xiu et al., 2011). Antigen-containing single-membrane vesicles with round or horse-shoe shapes were also detected. While it has been shown in dendritic cells that intralumenal vesicles are not required for MHCII loading (Bosch et al., 2013), multilamellar MIICs have also been reported (Unanue et al., 2016). These notions suggest that MIIC function is not bound to a certain vesicle morphology. Based on both the morphological and vesicle marker-based heterogeneity, we

propose that early peripheral antigen vesicles, eMIICs, are functional MIICs that are in transit (Fig. 6). While eMIICs might part off and fuse again or migrate as such to the perinuclear region for gradual maturation into MIICs, we suggest that they are functional throughout the pathway.

MATERIALS AND METHODS
For more information about reagents and antibodies, please see Table S1.

Cells and mice
A20 mouse lymphoma cells stably expressing a hen egg lysozyme (HEL)-specific IgM BCR (D1.3) (Williams et al., 1994) and 1E5T cells, kind gifts from Prof Facundo Batista (the Ragon Institute of MGH, MIT and Harvard, USA), stably expressing a transgenic TCR specific for HEL[108–116]/I-A^d (Adorini et al., 1993) were maintained in complete RPMI [cRPMI; RPMI 1640 with 2.05 mM L-glutamine supplemented with 10% fetal calf serum (FCS), 50 µM β-mercaptoethanol, 4 mM L-glutamine, 10 mM HEPES and 100 U/ml penicillin/streptomycin]. Cells were regularly examined for bacterial and fungal contaminations and tested for mycoplasma contaminations, but no other tests were run on the cell lines. Primary splenic B cells were isolated from 2–5-month-old male and female MD4 mice [C57BL/6-Tg(IghelMD4)4Ccg/J, The Jackson Laboratory] using a negative selection kit (StemCell Technologies, #19854). All animal experiments were approved by the Ethical Committee for Animal Experimentation in Finland, and were performed in adherence with the rules and regulations of the Finnish Act on Animal Experimentation (62/2006) and according to the 3R-principle (animal license numbers: 7574/04.10.07/2014, KEK/2018-2504-Mattila, 10727/2018).

Transfection
A20 D1.3 cells were transfected as previously described (Šuštar et al., 2018). Briefly, 2×10^6 cells were resuspended in 180 µl of 2S transfection buffer (5 mM KCl, 15 mM MgCl2, 15 mM HEPES, 50 mM sodium succinate, 180 mM Na$_2$HPO$_4$/ NaH$_2$PO$_4$ pH 7.2) containing 2 µg of plasmid and electroporated using an AMAXA electroporation machine (program X-005, Biosystem) in 0.2 cm gap electroporation cuvettes. Cells were then transferred to 2 ml of cRPMI to recover overnight. Rab5a–GFP plasmid was a kind gift from Prof. Johanna Ivaska (Turku Bioscience, University of Turku and Åbo Akademi University, Turku, Finland.).

B cell activation and visualisation of antigen vesicles by immunofluorescence

A20 D1.3 or isolated primary B cells were activated with 10 µg/ml of Alexa Fluor 647- or Rhodamine Red-X (RRx)-conjugated anti-mouse-IgM antibody (Jackson ImmunoResearch), unless indicated otherwise. Cells were labelled with fluorescently labelled anti-IgM for 10 min on ice, washed with PBS to remove excess unbound antigen and resuspended in imaging buffer (PBS, 10% FCS). When indicated, cells were also labelled with anti-MHCII conjugated to Alexa Fluor 488 on ice. After washing, cells were activated for different time points in an incubator (5% CO_2, 37°C) in a 12-wells PTFE diagnostic slide (Thermo Fisher Scientific, #10028210), coated with fibronectin, and fixed with 4% PFA 10 min at room temperature. Samples were blocked and permeabilised with blocking buffer (5% horse or donkey serum, 0.3% Triton X-100 in PBS) for 20 min at room temperature. After blocking, samples were stained with primary antibodies for 1 h at room temperature or 4°C overnight in staining buffer (1% BSA, 0.3% Triton X-100 in PBS), followed by washes with PBS and incubation with the secondary antibodies for 30 min at room temperature in PBS. Samples were mounted using FluoroMount-G containing DAPI (Thermo Fisher Scientific, #00495952).

Visualisation of antigen vesicles by live imaging

A20 D1.3 cells (1×10^6/ml) were labelled with 125 nM LysoTracker Deep Red (Thermo Fisher Scientific, #L12492) for 1 h in an incubator (5% CO_2, 37°C), washed with PBS and resuspended in cRPMI. Cells were then labelled with 10 µg/ml of donkey anti-mouse-IgM antibody conjugated to Alexa Fluor 488 on ice for 10 min and washed with cold PBS. For surface MHCII internalisation experiments, cells were stained on ice with anti-MHCII conjugated to Alexa Fluor 488 and 10 µl/ml donkey-anti mouse-IgM conjugated to RRx for 5 min and washed with cold PBS. Cells were resuspended in cold imaging buffer and seeded on four-well MatTek dishes on ice. After seeding, cells were activated at 37°C inside the environmental chamber of the microscope and image immediately.

Image acquisition and processing, spinning disk confocal microscopy

Images were acquired using a 3i CSU-W1 spinning disk equipped with 405, 488, 561 and 640 nm laser lines and 510–540, 580–654 and 672–712 nm filters and 63× Zeiss Plan-Apochromat objective. Hamamatsu sCMOS Orca Flash4 v2 |C11440-22CU (2048×2048 pixels, 1×1 binning) was used to image fixed samples unless otherwise indicated, and Photometrics Evolve 10 MHz Back Illuminated EMCCD (512×512 pixels, 1×1 binning) camera was used to image live samples.

All SDCM images were deconvolved with Huygens Essential version 16.10 (Scientific Volume Imaging, The Netherlands, http://svi.nl), using the CMLE algorithm, with a signal-to-noise ratio of 20 and 40 iterations. For SRRF, 20–50 images were acquired from one single plane using time-lapse mode and processed in Fiji ImageJ using the SRRF module.

Colocalisation analysis

Colocalisation analysis on spinning disk confocal microscope images was performed with Huygens Essential version 16.10 (Scientific Volume Imaging, The Netherlands, http://svi.nl), using optimised automatic thresholding. Colocalisation on SRRF images was performed with ImageJ using the Colocalisation Threshold tool. Graphs and statistics were prepared with GraphPad Prism (GraphPad Software, La Jolla, CA).

Analysis of antigen clustering

Cluster analysis of the deconvolved data was performed by batch processing in MATLAB R2018b (MathWorks). Binary masks were created from full volumes containing one cell using the method by Otsu. Objects were then segmented in 3D using the regionprops function. Only objects inside a circular mask were kept in order to exclude clusters from adjacent cells, for simplicity this was undertaken in 2D by manually overlaying the image with a circle. The MTOC channel was segmented in the same way and the cluster with the highest intensity value was identified as MTOC. The distances of each cluster to the MTOC was calculated from the centroid positions in 3D.

Graphs and statistics were prepared on GraphPad Prism. The scripts can be found on MattilaLab's GitHub (https://github.com/mattilalab/hernandez-perez-et-al-2019).

Structured illumination microscopy

The samples were prepared as above in the 'B cell activation and visualisation of antigen vesicles by immunofluorescence' section on fibronectin-coated MatTek dishes and mounted in Vectashield (Vector Laboratories) mounting medium. 3D structured illumination microscopy (SIM) Imaging was performed with GE Healthcare, DeltaVision OMX SR V4 with 60×/1.42 SIM Olympus Plan Apo N objective, front illuminated sCMOS cameras, and 488, 568 and 640 nm solid-state lasers by optical sectioning at 0.125 µm steps. The SIM reconstruction was performed with OMX Acquisition software version 3.70. (GE Healthcare, UK).

Antigen internalisation for flow cytometry

A20 D1.3 cells were stained on ice for 10 min with anti-IgM conjugated to biotin (Southern Biotech) or HEL–biotin and washed with PBS. Cells were incubated at 37C and 5% CO_2 at different time points. For time 0, the samples were kept on ice all the time after incubation, and stained with streptavidin-633 (LifeTechonologies #S-21375) for 20 min, before being washed and analysed. BD LSR Fortessa analyser equipped with four lasers (405, 488, 561 and 640 nm) was used. Data was analysed using FlowJo v10 (Tree Star).

Antigen internalisation and immunofluorescence

A20 D1.3 cells were stained on ice for 10 min with biotinylated anti-IgM antibody conjugated to Alexa Fluor 647 (labelled in-house) and washed with PBS. Cells were resuspended in Imaging Buffer (PBS, 10% FCS) and activated for different time points in an incubator (5% CO_2, 37°C) on fibronectin-coated 12-well microscope slide. After activation, slides were kept on ice to stop internalisation and stained with streptavidin–Alexa Fluor 488 (#S11223) for 10 min. Cells were washed with PBS and fixed with 4% PFA 10 min at room temperature. Samples were mounted using FluoroMount-G (Thermo Fisher Scientific, 00-4958-02).

DQ-Ova proteolysis reporter

DQ-Ovalbumin (Thermo Fisher Scientific, D12053) was biotinylated in-house with EZ-Link Maleimide–PEG2–biotin (Thermo Fisher Scientific, 21901BID). HEL from (Sigma-Aldrich, #L6876) was biotinylated using EZ-Link™ Sulfo-NHS-LC-LC-Biotin (Thermo Fisher Scientific, 21338). A20 D1.3 cells were first incubated with 10 µg/ml biotin-HEL or biotinylated anti-IgM (Southern Biotech) for 10 min on ice. After washing with PBS, cells were incubated for 5 min on ice with unlabelled streptavidin for immunofluorescence samples or Alexa Fluor 633-labelled streptavidin for flow cytometry samples, washed with PBS, and incubated 5 min on ice with biotinylated DQ-Ova. After three washes with PBS, cells were activated in an incubator (5% CO2, 37°C) to allow internalisation of the probe-linked antigen. After the activation, cells were placed on ice and analysed by flow cytometry immediately. For immunofluorescence samples, cells were activated on 12-well slides coated with fibronectin in the incubator, fixed with 4% PFA after activation, and stained as previously described. DQ-Ova was excited with 488 nm laser and measured with filters identical to Alexa Fluor 488 or GFP.

Assessment of low pH for flow cytometry

A20 D1.3 cells were stained on ice for 10 min with anti-IgM conjugated to Alexa Fluor 647 (5 µg/ml) and FITC (5 µg/ml) and washed with PBS. Cells were then incubated at 37°C and 5% CO_2 at different time points in a 96-well-plate for flow cytometry analysis. After incubation, cells were kept on ice and analysed using a BD LSR Fortessa analyser equipped with four lasers (405, 488, 561 and 640 nm). As time 0, the samples were kept on ice all the time. Data was analysed using FlowJo v10 (Tree Star).

Transmission electron microscopy

A20 D1.3 cells were activated with a mixture of 6 nm colloidal-gold conjugated goat anti-mouse IgM (Jackson ImmunoResearch, 115-195-075;

1:650 dilution) and 20 µg/ml Alexa Fluor 647-labelled donkey anti-mouse IgM F(ab′)$_2$ fragments (Jackson ImmunoResearch, 715-606-020) in imaging buffer (0.5 mM CaCl$_2$, 0.2 mM MgCl$_2$, 5.5 mM D-Glucose, 10% FBS in PBS) and placed on fibronectin (4 µg/ml)-coated glass coverslips (thickness #1) for 15 or 75 min. The cells were fixed with 2% glutaraldehyde (EM grade, Sigma-Aldirch, G7651) in 0.1 M sodium cacodylate buffer, pH 7.4, for 30 min at room temperature, and then washed twice for 3 min with 0.1 M sodium cacodylate buffer, pH 7.4. The samples were processed for TEM as described in Jokitalo et al. (2001); 60-nm-thick sections parallel to the cover slip were cut using a Leica EM Ultracut UC7 ultramicrome (Leica Mikrosysteme GmbH, Austria). The electron micrographs were post stained with uranyl acetate and lead citrate, and imaged with a Jeol JEM 1400 transmission electron microscope (Jeol Ltd., Tokyo, Japan) equipped with a bottom mounted CCD camera (Orius SC 1000B, Gatan Inc., Pleasanton, CA) and Jeol JEM-1400 Plus equipped with an OSIS Quemesa bottom-mounted CCD camera (EMSIS, Germany), both operating at 80 kV.

DAB endosome ablation
The endosome ablation assay was adapted from Pond and Watts (1999). A20 D1.3 cells (10^7/ml) were incubated in FCS-free RPMI for 45 min at 37°C. Cells were surface-stained on ice with 10 µg/ml of anti-IgM conjugated to biotin (Southern Biotech) for 10 min, followed by one PBS wash. Then, cells were incubated with streptavidin–HRP for 10 min on ice and washed twice with PBS. Internalisation of anti-IgM–HRP was initiated by incubation at 37°C and 5% CO$_2$ for different times (10, 20 and 40 min). After that, vesicle trafficking was stopped by incubation on ice and anti-IgM–HRP-containing endosomes were ablated by addition of 0.1 mg/ml DAB (Santa Cruz Biotechnology, sc-24982) and 0.025% H$_2$O$_2$ in freshly prepared DAB buffer (70 mM NaCl, 20 mM HEPES, 2 mM CaCl2 and 50 mM ascorbic acid) for 30 min on ice in the dark. Ascorbic acid is a membrane-impermeable molecule that acts as a radical scavenger inhibiting extracellular HRP activity to avoid DAB deposits on the plasma membrane. As a control, cells were incubated in DAB buffer with 0.1 mg/ml DAB, but without HRP or without H$_2$O$_2$. Cells were then washed three times with PBS containing 1% BSA and kept on ice. Viability after the endosome ablation, assessed by Trypan Blue staining, was 95–98%.

Antigen presentation measured by ELISA
After endosome ablation, A20 D1.3 cells were incubated with 10 µg/ml of HEL for 1 h at 37°C in cRPMI. After 1 h, cells were washed and resuspend in cRPMI. A20 D1.3 B cells were mixed with 1E5T cells (ratio 2:1) and incubated at 37°C and 5% CO$_2$ overnight. IL-2 secretion levels were measured the next day by ELISA on half-area 96-well plates coated with capture antibodies (anti-IL-2) for 1 h at 37°C in 25 µl of PBS. Non-specific binding sites were blocked overnight at 4°C in 150 µl of blocking buffer (PBS, 1% BSA). Appropriate dilutions of 50 µl supernatant samples in cRPMI were added to the ELISA plate for an 1–2 h incubation at 37°C. Biotin-conjugated detection antibodies (anti-IL-2–biotin) in 50 µl of blocking buffer were added for 1 h at room temperature followed by 50 µl alkaline phosphatase (AP)–streptavidin in blocking buffer for 1 h at room temperature. In between all incubation steps, plates were washed with 150 µl washing buffer (PBS with 0.05% Tween-20). The final wash was completed with two washes with 150 µl of water. Finally, 50 µl of pNPP solution was added and the optical density (OD) was measured at 405 nm. Typical time for AP–substrate incubation before measurement was ∼10–20 min at room temperature, before reaching signal saturation.

All ELISA samples were run in duplicates, and OD values were averaged and blank background was subtracted. All samples were normalised to values of the control cells (100%) and data is presented as mean±s.d. of three experiments.

Statistical analysis and illustrations
Statistical significances were calculated using unpaired Student's t-test assuming normal distribution of the data. Statistical values are denoted as: *$P<0.05$, **$P<0.01$, ***$P<0.001$, ****$P<0.0001$. Graphs were created in GraphPad Prism 6 and illustrations were created with BioRender. Figure formatting was undertaken on Inkscape v.092.2.

References
Adler, L. N., Jiang, W., Bhamidipati, K., Millican, M., Macaubas, C., Hung, S. C. and Mellins, E. D. (2017). The other function: class II-restricted antigen presentation by B cells. Front. Immunol. 8, 319. doi:10.3389/fimmu.2017.00319

Adorini, L., Guéry, J. C., Fuchs, S., Ortiz-Navarrete, V., Hämmerling, G. J. and Momburg, F. (1993). Processing of endogenously synthesized hen egg-white lysozyme retained in the endoplasmic reticulum or in secretory form gives rise to a similar but not identical set of epitopes recognized by class II-restricted T cells. J. Immunol. 151, 3576-3586.

Aluvihare, V. R., Khamlichi, A. A., Williams, G. T., Adorini, L. and Neuberger, M. S. (1997). Acceleration of intracellular targeting of antigen by the B-cell antigen receptor: importance depends on the nature of the antigen-antibody interaction. EMBO J. 16, 3553-3562. doi:10.1093/emboj/16.12.3553

Amigorena, S., Drake, J. R., Webster, P. and Mellman, I. (1994). Transient accumulation of new class II MHC molecules in a novel endocytic compartment in B lymphocytes. Nature 369, 113-120. doi:10.1038/369113a0

Barroso, M., Tucker, H., Drake, L., Nichol, K. and Drake, J. R. (2015). Antigen-B cell receptor complexes associate with intracellular major histocompatibility complex (MHC) class II molecules. J. Biol. Chem. 290, 27101-27112. doi:10.1074/jbc.M115.649582

Bosch, B., Berger, A. C., Khandelwal, S., Heipertz, E. L., Scharf, B., Santambrogio, L. and Roche, P. A. (2013). Disruption of multivesicular body vesicles does not affect major histocompatibility complex (MHC) class II-peptide complex formation and antigen presentation by dendritic cells. J. Biol. Chem. 288, 24286-24292. doi:10.1074/jbc.M113.461996

Castellino, F. and Germain, R. N. (1995). Extensive trafficking of MHC class II-invariant chain complexes in the endocytic pathway and appearance of peptide-loaded class II in multiple compartments. Immunity 2, 73-88. doi:10.1016/1074-7613(95)90080-2

Chen, K.-E., Healy, M. D. and Collins, B. M. (2019). Towards a molecular understanding of endosomal trafficking by Retromer and Retriever. Traffic 20, 465-478. doi:10.1111/tra.12649

Clotworthy, M. and Traynor, D. (2006). On the effects of cycloheximide on cell motility and polarisation in Dictyostelium discoideum. BMC Cell Biol. 7, 5. doi:10.1186/1471-2121-7-5

Darvishi, E. and Woldemichael, G. M. (2016). Cycloheximide inhibits actin cytoskeletal dynamics by suppressing signaling via RhoA. J. Cell. Biochem. 117, 2886-2898. doi:10.1002/jcb.25601

Davidson, H. W., West, M. A. and Watts, C. (1990). Endocytosis, intracellular trafficking, and processing of membrane IgG and monovalent antigen/membrane IgG complexes in B lymphocytes. *J. Immunol.* **144**, 4101-4109.

Delevoye, C., Marks, M. S. and Raposo, G. (2019). Lysosome-related organelles as functional adaptations of the endolysosomal system. *Curr. Opin. Cell Biol.* **59**, 147-158. doi:10.1016/j.ceb.2019.05.003

Denzin, L. K., Fallas, J. L., Prendes, M. and Yi, W. (2005). Right place, right time, right peptide: DO keeps DM focused. *Immunol. Rev.* **207**, 279-292. doi:10.1111/j.0105-2896.2005.00302.x

Gondré-Lewis, T. A., Moquin, A. E. and Drake, J. R. (2001). Prolonged antigen persistence within nonterminal late endocytic compartments of antigen-specific B lymphocytes. *J. Immunol.* **166**, 6657-6664. doi:10.4049/jimmunol.166.11.6657

Gustafsson, N., Culley, S., Ashdown, G., Owen, D. M., Pereira, P. M. and Henriques, R. (2016). Fast live-cell conventional fluorophore nanoscopy with ImageJ through super-resolution radial fluctuations. *Nat. Commun.* **7**, 12471. doi:10.1038/ncomms12471

Henry, L. and Sheff, D. R. (2008). Rab8 regulates basolateral secretory, but not recycling, traffic at the recycling endosome. *Mol. Biol. Cell* **19**, 1815-2348. doi:10.1091/mbc.e07-09-0902

Huotari, J. and Helenius, A. (2011). Endosome maturation. *EMBO J.* **30**, 3481-3500. doi:10.1038/emboj.2011.286

Hutagalung, A. H. and Novick, P. J. (2011). Role of Rab GTPases in membrane traffic and cell physiology. *Physiol. Rev.* **91**, 119-149. doi:10.1152/physrev.00059.2009

Jiang, W., Strohman, M. J., Somasundaram, S., Ayyangar, S., Hou, T., Wang, N. and Mellins, E. D. (2015). pH-susceptibility of HLA-DO tunes DO/DM ratios to regulate HLA-DM catalytic activity. *Sci. Rep.* **5**, 17333. doi:10.1038/srep17333

Jokitalo, E., Cabrera-Poch, N., Warren, G. and Shima, D.T. (2001). Golgi clusters and vesicles mediate mitotic inheritance independently of the endoplasmic reticulum. *J. Cell Biol.* **154**, 317-330. doi:10.1083/jcb.200104073

Karlsson, L. (2005). DM and DO shape the repertoire of peptide-MHC-class-II complexes. *Curr. Opin. Immunol.* **17**, 65-70. doi:10.1016/j.coi.2004.11.003

Kirkham, M., Fujita, A., Chadda, R., Nixon, S. J., Kurzchalia, T. V., Sharma, D. K., Pagano, R. E., Hancock, J. F., Mayor, S. and Parton, R. G. (2005). Ultrastructural identification of uncoated caveolin-independent early endocytic vehicles. *J. Cell Biol.* **168**, 465-476. doi:10.1083/jcb.200407078

Lankar, D., Vincent-Schneider, H., Briken, V., Yokozeki, T., Raposo, G. and Bonnerot, C. (2002). Dynamics of major histocompatibility complex class II compartments during B cell receptor-mediated cell activation. *J. Exp. Med.* **195**, 461-472. doi:10.1084/jem.20011543

Manders, E. M. M., Verbeek, F. J. and Aten, J. A. (1993). Measurement of co-localization of objects in dual-colour confocal images. *J. Microsc.* **169**, 375-382. doi:10.1111/j.1365-2818.1993.tb03313.x

Martinez-Martin, N., Maldonado, P., Gasparrini, F., Frederico, B., Aggarwal, S., Gaya, M., Tsui, C., Burbage, M., Keppler, S. J., Montaner, B. et al. (2017). A switch from canonical to noncanonical autophagy shapes B cell responses. *Science* **355**, 641-647. doi:10.1126/science.aal3908

Mellins, E. D. and Stern, L. J. (2014). HLA-DM and HLA-DO, key regulators of MHC-II processing and presentation. *Curr. Opin. Immunol.* **26**, 115-122. doi:10.1016/j.coi.2013.11.005

Oksvold, M. P., Pedersen, N. M., Forfang, L. and Smeland, E. B. (2012). Effect of cycloheximide on epidermal growth factor receptor trafficking and signaling. *FEBS Lett.* **586**, 3575-3581. doi:10.1016/j.febslet.2012.08.022

Pond, L. and Watts, C. (1999). Functional early endosomes are required for maturation of major histocompatibility complex class II molecules in human B lymphoblastoid cells. *J. Biol. Chem.* **274**, 18049-18054. doi:10.1074/jbc.274.25.18049

Rink, J., Ghigo, E., Kalaidzidis, Y. and Zerial, M. (2005). Rab conversion as a mechanism of progression from early to late endosomes. *Cell* **122**, 735-749. doi:10.1016/j.cell.2005.06.043

Roche, P. A. and Furuta, K. (2015). The ins and outs of MHC class II-mediated antigen processing and presentation. *Nat. Rev. Immunol.* **15**, 203-216. doi:10.1038/nri3818

Siemasko, K., Eisfelder, B. J., Williamson, E., Kabak, S. and Clark, M. R. (1998). Cutting edge: signals from the B lymphocyte antigen receptor regulate MHC class II containing late endosomes. *J. Immunol.* **160**, 5203-5208.

Stoorvogel, W., Oorschot, V. and Geuze, H. J. (1996). A novel class of clathrin-coated vesicles budding from endosomes. *J. Cell Biol.* **132**, 21-33. doi:10.1083/jcb.132.1.21

Šuštar, V., Vainio, M. and Mattila, P. K. (2018). Visualization and quantitative analysis of the actin cytoskeleton upon b cell activation. *Methods Mol. Biol.* **1707**, 243-257. doi:10.1007/978-1-4939-7474-0_18

Tsui, C., Martinez-Martin, N., Gaya, M., Maldonado, P., Llorian, M., Legrave, N. M., Rossi, M., MacRae, J. I., Cameron, A. J., Parker, P. J. et al. (2018). Protein kinase c-beta dictates b cell fate by regulating mitochondrial remodeling, metabolic reprogramming, and heme biosynthesis. *Immunity* **48**, 1144-1159.e5. doi:10.1016/j.immuni.2018.04.031

Unanue, E. R., Turk, V. and Neefjes, J. (2016). Variations in MHC Class II antigen processing and presentation in health and disease. *Annu. Rev. Immunol.* **34**, 265-297. doi:10.1146/annurev-immunol-041015-055420

van Lith, M., van Ham, M., Griekspoor, A., Tjin, E., Verwoerd, D., Calafat, J., Janssen, H., Reits, E., Pastoors, L. and Neefjes, J. (2001). Regulation of MHC class II antigen presentation by sorting of recycling HLA-DM/DO and class II within the multivesicular body. *J. Immunol.* **167**, 884-892. doi:10.4049/jimmunol.167.2.884

Vascotto, F., Lankar, D., Faure-André, G., Vargas, P., Diaz, J., Le Roux, D., Yuseff, M.-I., Sibarita, J.-B., Boes, M., Raposo, G. et al. (2007a). The actin-based motor protein myosin II regulates MHC class II trafficking and BCR-driven antigen presentation. *J. Cell Biol.* **176**, 1007-1019. doi:10.1083/jcb.200611147

Vascotto, F., Le Roux, D., Lankar, D., Faure-André, G., Vargas, P., Guermonprez, P. and Lennon-Duménil, A.-M. (2007b). Antigen presentation by B lymphocytes: how receptor signaling directs membrane trafficking. *Curr. Opin. Immunol.* **19**, 93-98. doi:10.1016/j.coi.2006.11.011

Vonderheit, A. and Helenius, A. (2005). Rab7 associates with early endosomes to mediate sorting and transport of Semliki forest virus to late endosomes. *PLoS Biol.* **3**, e233. doi:10.1371/journal.pbio.0030233

Wandinger-Ness, A. and Zerial, M. (2014). Rab proteins and the compartmentalization of the endosomal system. *Cold Spring Harb. Perspect. Biol.* **6**, a022616. doi:10.1101/cshperspect.a022616

West, M. A., Lucocq, J. M. and Watts, C. (1994). Antigen processing and class II MHC peptide-loading compartments in human B-lymphoblastoid cells. *Nature* **369**, 147-151. doi:10.1038/369147a0

Whitmire, J. K., Asano, M. S., Kaech, S. M., Sarkar, S., Hannum, L. G., Shlomchik, M. J. and Ahmed, R. (2009). Requirement of b cells for generating CD4+ T cell memory. *J. Immunol.* **182**, 1868-1876. doi:10.4049/jimmunol.0802501

Williams, G.T., Peaker, C.J., Patel, K.J. and Neuberger, M.S (1994). The alpha/beta sheath and its cytoplasmic tyrosines are required for signaling by the B-cell antigen receptor but not for capping or for serine/threonine-kinase recruitment. *Proc. Natl. Acad. Sci. U.S.A.* **91**, 474-478. doi:10.1073/pnas.91.2.474

Xiu, F., Côté, M.-H., Bourgeois-Daigneault, M.-C., Brunet, A., Gauvreau, M.-É., Shaw, A. and Thibodeau, J. (2011). Cutting edge: HLA-DO impairs the incorporation of HLA-DM into exosomes. *J. Immunol.* **187**, 1547-1551. doi:10.4049/jimmunol.1100199

Yonemura, Y., Li, X., Müller, K., Krämer, A., Atigbire, P., Mentrup, T., Feuerhake, T., Kroll, T., Shomron, O., Nohl, R. et al. (2016). Inhibition of cargo export at ER exit sites and the trans-Golgi network by the secretion inhibitor FLI-06. *J. Cell Sci.* **129**, 3868-3877. doi:10.1242/jcs.186163

Yuseff, M.-I., Reversat, A., Lankar, D., Diaz, J., Fanget, I., Pierobon, P., Randrian, V., Larochette, N., Vascotto, F., Desdouets, C. et al. (2011). Polarized secretion of lysosomes at the B cell synapse couples antigen extraction to processing and presentation. *Immunity* **35**, 361-374. doi:10.1016/j.immuni.2011.07.008

Yuseff, M.-I., Pierobon, P., Reversat, A. and Lennon-Duménil, A.-M. (2013). How B cells capture, process and present antigens: a crucial role for cell polarity. *Nat. Rev. Immunol.* **13**, 475-486. doi:10.1038/nri3469